A simplified non-linear modelling strategy to generate fragility curves for old masonry buildings

Alessandro Stocchi, Cédric Giry, Sophie Capdevielle, Irmela Zentner, Emmanuelle Nayman, Frédéric Ragueneau

Version of Record: https://www.sciencedirect.com/science/article/pii/S0045794921001012
Manuscript_26d8382323ea90d78de81d9738b2138f

A simplified non-linear modelling strategy to generate fragility curves for old masonry buildings

Alessandro Stocchi[a], Cédric Giry[a], Sophie Capdevielle[a,b,*], Irmela Zentner[c], Emmanuelle Nayman[d], Frédéric Ragueneau[a]

[a] *Université Paris-Saclay, ENS Paris-Saclay, CNRS, LMT - Laboratoire de Mécanique et Technologie, 91190, Gif-sur-Yvette, France*
[b] *Université Grenoble Alpes, CNRS, Grenoble INP, 3SR, 38000 Grenoble, France*
[c] *EDF R&D Lab Paris-Saclay 91120 Palaiseau, France*
[d] *EDF-Direction Industrielle, Aix-en-Provence, France*

Abstract

In the context of historical seismology, studying the behaviour of historic masonry buildings is of great importance, as they are witnesses of past events. While interesting methods can be found in the literature to assess the seismic vulnerability of masonry structures subject to strong earthquakes, the topic of moderate seismicity, as encountered in many European countries, is still to be investigated. The present work proposes a global methodology to build fragility curves for existing masonry buildings. An efficient computational method to address the non-linear response of masonry structures is presented. The method is based on the modal decomposition of the structural response. An equivalent non-linear single degree of freedom oscillator is identified for the main modes. The modelling strategy enables to carry out numerous computations with a low computational effort, allowing for a probabilistic approach. To build fragility curves, a damage indicator based on the frequency shift is chosen. To validate the proposed approach, the simplified model of a real masonry building is compared to a full non-linear time history analysis. The method is eventually illustrated by the derivation of fragility curves for industrial masonry buildings.

Keywords: Masonry, Fragility Functions, Historical seismology, Damage

1. Introduction

For design purposes, a level of seismic intensity based on the known past earthquakes is defined. In moderate seismic regions, the instrumental seismology is not old

*Corresponding author
Email addresses: Alessandro.Stocchi@emi.fraunhofer.de (Alessandro Stocchi), cedric.giry@ens-paris-saclay.fr (Cédric Giry), sophie.capdevielle@univ-grenoble-alpes.fr (Sophie Capdevielle), irmela.zentner@edf.fr (Irmela Zentner), emmanuelle.naymann@edf.fr (Emmanuelle Nayman), frederic.ragueneau@ens-paris-saclay.fr (Frédéric Ragueneau)

enough to rely on measured earthquakes only. The definition of a macro-seismic intensity for historical earthquakes is needed, often based on archival testimony. However, the data available to quantify these historical earthquakes may not be sufficient. In particular, if no considerable damage is reported in the identified historical documents, the uncertainties related to the macro-seismic intensity and to the epicentre location of the earthquake may be high.

Recent methodologies [1] propose to introduce structural analyses in the process of defining the macroseismic intensity of historical earthquakes. The main idea is to update the distribution of intensities or magnitudes of the considered earthquake by means of a Bayesian approach, combining historical data, fragility curves and in-situ observed damages. This approach is very promising in the context of low to moderate seismic activity, such as encountered in France, associated to a large amount of old structures as well as cultural heritage. The method can be used as a way to reduce the uncertainties associated to the the process of assigning magnitudes to historical earthquakes. For this purpose, the building stock is classified in a number of typologies for which fragility curves are computed [2, 3]. This paper focuses on the derivation of such fragility curves for old masonry buildings subject to low to moderate earthquakes.

The structural analysis of historical masonry buildings can be handled with different numerical strategies as presented in [4] and [5]. A global methodology to derive fragility functions for masonry structures can be found in [6], along with a set of fragility curves for specific building typologies. Macro-element models are commonly used for the generation of fragility curves [5, 7]. An exemple of numerical limit analysis based on macro-elements can also be found in [8]. Nevertheless, finite element (FE) based modelling has several advantages, as explained below, if adequate amount of computational resources [9] is available. FE models are used to address the seismic vulnerability of historical structures exhibiting several local modes [10, 11, 12], or also within the framework of limit analysis [13, 14]. The macro-element approach is very interesting for a relatively high seismic level, when a global state of damage with large macro-cracks is reached for the structure. In the context of low seismic activity however, the seismic load generally leads to low damages. The cracks are rather small and distributed in the structures. In this case, a FE computation is more relevant for the structural analysis, and several masonry models have been developed based on a continuous approach [15, 16, 17, 18]. To build fragility curves based on this approach, a large number of computations must be carried out for a structure typology. Indeed, uncertainties on the structure as well as on the material must be taken into account. Thus, an efficient numerical method must be adopted.

In this paper, a global modelling strategy is presented, based on the modal decomposition of the structure and the identification of non-linear single degree of freedom (NLSDOF) oscillators. Despite its simplicity and the use of certain hypotheses, non-linear simple oscillators allow to obtain an accurate global response and information regarding the damage state of the structure considering global indicators. The method is suitable for structures for which local modes are not preponderant or do not lead to strong damage. After a detailed presentation of the developed modelling strategy, the method is applied to the case of a real historical masonry structure. The computed response is first compared to a full 3D non linear time history analysis (NLTHA) of the building. The probabilistic framework is then addressed. From the computed struc-

tural responses, the method used to derive fragility curves is presented. The definition of a structural damage criterion is discussed, and fragility curves are derived for the considered case-study.

2. Modelling strategy

The purpose of this work is to derive fragility curves for historical buildings for cases where low damage is expected. To take into account the spatial and material variability of structures within a typology, a large number of computations are needed. In order to overcome the computational cost of such studies, specific tools need to be used. A simplified modelling strategy of the non-linear response of the structure is developed here. The overall methodology is based on the displacement modal decomposition, described in section 2.1. A single degree of freedom oscillator is identified for each mode of the considered structure by a pushover-like analysis. A 3D finite element model of the structure is used to compute its response. The model is described in section 2.2, along with the corresponding developed numerical tools. The simplified model and the identification of the parameters governing the response of the simple oscillators are finally explained in section 2.3.

2.1. A simplified method to compute the nonlinear structural response

To carry out a fragility analysis accounting for the variability of the considered building and seismic loading properties, efficient numerical tools are needed. In what follows, the simplified modelling strategy of the nonlinear response of the structure based on the modal decomposition of the response is presented.

The displacement field $\boldsymbol{U}(t)$ can be expressed on the modal basis according to Eq. (1). $\boldsymbol{\phi}_i$ and $q_i(t)$ are respectively the eigenvector and the modal displacement of the mode i. $\boldsymbol{P}$ consequently denotes the matrix of the modal basis.

$$\boldsymbol{U}(t) = \sum_i q_i(t)\,\boldsymbol{\phi}_i = \boldsymbol{P}\,\boldsymbol{q}(t) \tag{1}$$

In the context of low to moderate damage for regular buildings, the mode shape is assumed to remain unaltered. Furthermore, the energies stored or dissipated in the system are considered to evolve independently for each mode. This framework is similar to the one proposed for modal pushover analysis [19, 20]. The free energy ψ in the structure is decomposed on each mode according to Eq. (2), where V_i are the internal variables associated to the chosen model of mode i (damage, plasticity...):

$$\psi(\boldsymbol{U}, \dots) = \sum_i \psi_i(q_i, V_i) \tag{2}$$

The dissipation $\mathcal{D}_{vis}$ associated to viscous damping is also considered decomposed on each mode shape as displayed in Eq. (3). c_i is the damping coefficient for mode i, modelled as a linear viscous damper. The dissipated energy is eventually written in terms of the natural vibration frequency of mode i ω_i and the corresponding viscous

damping ratio ξ_i. Considering the modal displacement responding as a single degree of freedom vibrating in its linear elastic range, $c_i = 2\,\xi_i\,\omega_i$, we have:

$$\mathcal{D}_{vis}\left(\dot{\boldsymbol{U}},\dots\right) = \sum_i \mathcal{D}_{visi}\left(\dot{q}_i\right) = \sum_i \frac{1}{2} c_i\,\dot{q}_i^2 = \sum_i \xi_i\,\omega_i\,\dot{q}_i^2 \tag{3}$$

Since the mass matrix $\boldsymbol{M}$ does not evolve, the kinetic energy $\mathcal{T}$ can be decomposed independently on each mode (Eq. (4)).

$$\mathcal{T}\left(\dot{\boldsymbol{U}},\dots\right) = \sum_i \mathcal{T}_i\left(\dot{q}_i\right) = \sum_i \frac{1}{2}\boldsymbol{\phi}_i^T\,\boldsymbol{M}\boldsymbol{\phi}_i\dot{q}_i^2 = \sum_i \frac{1}{2} m_i\dot{q}_i^2 \tag{4}$$

Furthermore, with $a_{g_k}(t)$ denoting the acceleration in the direction k and $\boldsymbol{\Delta_k}$ the vector associated to the direction k, the mathematical expression of the generalized force Q_i associated to the seismic loading on mode i can be expressed as :

$$Q_i = -\sum_k \boldsymbol{\phi}_i^T\,\boldsymbol{M}\boldsymbol{\Delta_k} a_{g_k}(t) \tag{5}$$

Let's introduce $\mathcal{L}$ the Lagrangian of the structure, equal to $\mathcal{L} = \mathcal{T} - \psi$. According to the Lagrange equations, the equation of equilibrium on each mode reads:

$$\frac{d}{dt}\left(\frac{\partial\mathcal{L}}{\partial\dot{q}_i}\right) - \left(\frac{\partial\mathcal{L}}{\partial q_i}\right) = Q_i - \left(\frac{\partial\mathcal{D}_{vis}}{\partial\dot{q}_i}\right) \tag{6}$$

That is to say:

$$m_i\,\ddot{q}_i\left(t\right) + 2\,\xi_i\,\omega_i\,\dot{q}_i\left(t\right) + f_{int}^i\left(q_i\left(t\right)\right) = -\sum_k \boldsymbol{\phi}_i^T\,\boldsymbol{M}\boldsymbol{\Delta_k} a_{g_k}(t) \tag{7}$$

$f_{int}^i\left(q_i\left(t\right)\right)$ is the internal force associated to mode i. Its expression derives from the free energy ψ_i (Eq. (8)):

$$F_{int}^i\left(q_i\left(t\right)\right) = \frac{\partial\psi}{\partial q_i} = \frac{\partial\psi_i}{\partial q_i} \tag{8}$$

The model used to compute the modal response (ie $F_{int}^i\left(q_i\left(t\right)\right)$) can be more or less complex according to the nonlinear phenomena considered. Section 2.3 describes the model chosen for the present study. It is identified thanks to the global response of the structure submitted to a displacement field proportional to the mode shape. This global response is computed thanks to a 3D finite element analysis of the structure, as described in the following section.

2.2. 3D finite element analysis of the structure

In this section, the 3D numerical model used to compute the structural response is described. This model will be used to identify the simplified model behaviour in section 2.3. The numerical tools to generate a parametric mesh are developed first. The parametric mesh allows for handy propagation of uncertainties on geometrical parameters of the studied structures, using the SalomeMeca platform [21]. Then, the nonlinear material model to compute the masonry structural behaviour is explained.

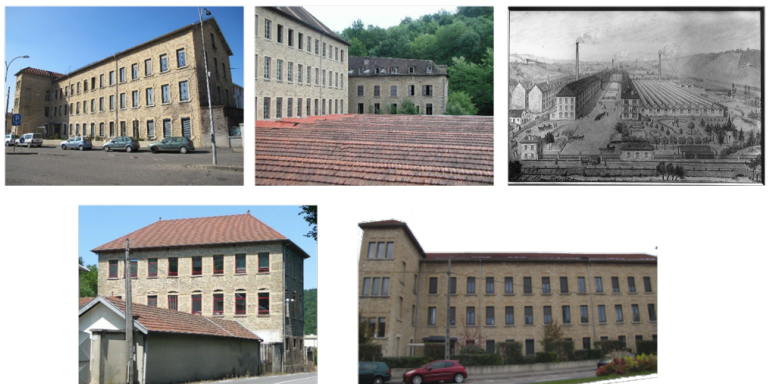

Figure 1: Examples of French historical industrial buildings in masonry from the 19th century. Pictures from https://collections.isere.fr/ and [24]

The output of the global response used for the identification of the SDOF parameters are eventually described.

2.2.1. A parametric mesh to account for structural uncertainties

In order to develop a tool capable of describing different buildings of a same typology, a parametric mesh generator has been developed. With the help of the Salome mesh module [21], it is possible to generate a parameterised mesh. In this framework, the following variables have been considered: base length to width ratio, storey height, openings distribution, openings to wall ratio. These parameters have been chosen according to the influence they can have in the seismic response of the structure, such as the modal analysis, or the development of the nonlinearities. This choice has been guided by the recommendation of the Perpetuate project [5] and the authors' experience [22].

The code generates a mesh with 4 and/or 3 nodes multilayer shell elements, as structured as possible. The NETGEN mesh engine is used [21]. The mesh refinement is adapted according to the case study in order to reach an optimum between computational resources and quality of output in a probabilistic framework (i.e. a good description of the main modal shapes and a good estimation of the associated eigenfrequencies).

In this paper, the case of the industrial building typology will be addressed to illustrate the proposed methodology. Figure 1 displays several examples of buildings, all related to textile industry in France in the nineteenth century [23]. Figure 2 shows one result of the mesh generator for the industrial building typology. For this example of the industrial building typology, the global size (length, width and height of the building) is different for each sample. As the opening distribution does not seem to vary much from a building to another for this typology, the variability of regularity or amount of perforation were not considered as stochastic variables for the present study.

The material models are described below.

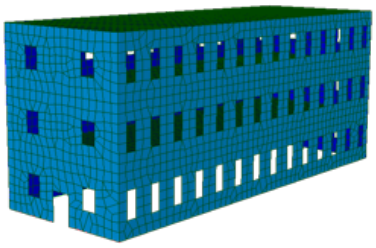

Figure 2: Example of a randomly generated mesh for the industrial building typology.

2.2.2. *Material modelling*

The masonry used for the buildings stock in the region of interest is mainly characterized by a moderate aspect ratio, leading to a "weak" orthotropy. An isotropic elastic model is thus considered to describe the linear behaviour of the masonry. When subject to a monotonic loading, the nonlinear behaviour of the masonry is mainly characterized by a progressive degradation of the stiffness with negligible dissipation by hysteretic phenomena. These nonlinearities are well-reproduced with a damage model. Due to the type of masonry (heterogeneous or with moderate aspect ratio), damage is also considered as isotropic. The Mazars damage model [25] available in Code_Aster [26] has been used. This model is used to compute the response of the structure to a pushover-like monotonic loading. Thus, the unilateral effect as well as complex hysteretic phenomena due to friction do not need to be described by the model. Examples of application of Mazars damage model to masonry FE modelling can also be found in the existing literature [27], and [28] for an application of the model with pushover analysis over an old masonry tower.

The main equations of the model and the associated parameters are recalled in Eq. (9) to (12).

The constitutive law is defined as:

$$\boldsymbol{\sigma} = (1 - D) \, . \, [\lambda . \mathrm{Trace} \, (\boldsymbol{\varepsilon}) \, . \boldsymbol{I} + 2 . \mu . \boldsymbol{\varepsilon}] \tag{9}$$

D is the scalar damage variable, $\boldsymbol{\sigma}$ denotes the stress tensor and $\boldsymbol{\varepsilon}$ the strain tensor. λ and μ are the classical Lamé parameters. The threshold function φ associated to damage is driven by an equivalent strain ε_{eq} depending on the principal positive strains (Eq. (10)).

$$\varphi = \varepsilon_{eq} - \kappa \, (D) \tag{10}$$

κ is a history variable corresponding to the maximum value reached for ε_{eq} along history. It is equal to the strain at damage threshold ε_{D_0} for $D = 0$ and up to damage initiation. D is finally computed according to Eq. (11) and (12).

$$D = \alpha_C^{\beta} . D_C + \alpha_T^{\beta} . D_T \tag{11}$$

$$D_{C,T} = 1 - \frac{(1 - A_{C,T})\,\varepsilon_{D_0}}{\varepsilon_{eq}} - A_{C,T} \exp\left(-B_{C,T}\left(\varepsilon_{eq} - \varepsilon_{D_0}\right)\right) \tag{12}$$

A_C, B_C are parameters that define the evolution law in compression and A_T, B_T are parameters that define the evolution law in tension. The variables α_C and α_T are computed thanks to the effective stress tensor. They weight the part of damage D_C due to compression loading and D_T due to tension loading. β is a parameter that has been originally introduced to better describe the response of quasi-brittle materials for shear loading.

The constitutive laws are calibrated upon available data [29] , [22] .

For the simulation of the different structural elements, multilayer shell elements are used. The nonlinear behaviour described above is used to model the vertical elements representing the walls. A linear homogenized behaviour is considered for horizontal elements modelling floors and roof, to optimize the computational time.

2.2.3. Structural global response

The 3D FE model described above is used to compute the structural response. The computations of the 3D FE model have been performed with Code_Aster [26]. After generating a mesh corresponding to a typology of building, a modal analysis of the structure is carried out. An example of response for one building for the main modes in the x and y directions is displayed in figure 3. These modes are global modes of the structure. The particular deformed shape that can be observed in figure 3 is due to the stiffness of the floors, and to the relatively high number of openings.

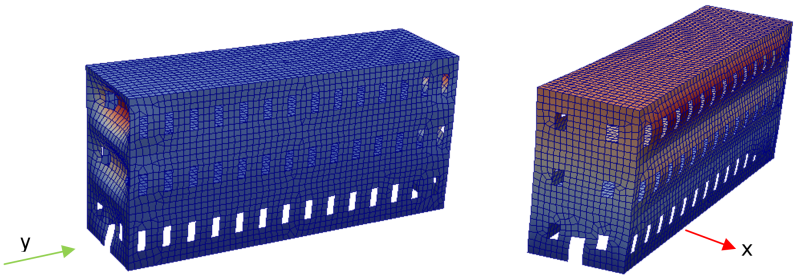

Figure 3: Modal analysis displacement fields for principal modes in y and x direction.

A nonlinear pushover-like analysis is then performed for the first natural modes. Previous studies [11, 30] have successfully used this pushover approach to compute the response of masonry structures. The structure is submitted to a displacement field proportional to the mode shape: $\boldsymbol{\delta}_{load} = \lambda\,\boldsymbol{\phi}_i$. This means that the displacement control coefficient λ is given by the distribution of displacements obtained with the modal analysis, and can be directly identified as the modal displacement q_i defined in Eq. (1). To identify the internal force F^i_{int}, a conversion factor is used. By considering the

direction k as the main direction of the considered mode, F^i_{int} can be identified with the base shear force V_{b_k} in direction k, and the modal participation factor p_{i_k} of mode i in the direction k. Eq. (13) provides this coefficient for the example of a linear behaviour for mode i:

$$V_{b_k} = \boldsymbol{\Delta}_k^{\mathrm{T}} \left(\lambda \boldsymbol{K} \boldsymbol{\phi}_i\right) = \lambda \sum_i p_{i_k} \boldsymbol{\phi}_i^T \boldsymbol{K} \boldsymbol{\phi}_i = p_{i_k} k_i \lambda \rightarrow \; F^i_{int}\left(q_i\right) = k_i q_i = \frac{V_{b_k}}{p_{i_k}} \tag{13}$$

The computed response (V_{b_k}, q_i) is then used to identify the parameter of a single degree of freedom (SDOF) model for each mode. This model and the identification process are described in what follows.

2.3. Identification of the single degree of freedom system behaviour for each mode

2.3.1. Damage model used for the single degree of freedom system

For the nonlinear SDOF behaviour of a mode, a unilateral damage model is considered. Eq. (14) gives the free energy of this model. k_i is the initial modal stiffness. D_i^+ and D_i^- represent the damage associated with the positive and negative modal displacements, respectively.

$$\psi_i\left(q_i, D_i^+, D_i^-\right) = \frac{1}{2} k_i \left(1 - D_i^+\right) < q_i >_+^2 + \frac{1}{2} k_i \left(1 - D_i^-\right) < q_i >_-^2 \tag{14}$$

The internal force is obtained by deriving the free energy according to the modal displacement (Eq. (15)).

$$f^i_{int}\left[q_i\left(t\right)\right] = \frac{\partial \psi_i}{\partial q_i} = k_i \left(1 - D_i^+\right) < q_i >_+ + k_i \left(1 - D_i^-\right) < q_i >_- \tag{15}$$

A threshold function is defined in Eq. (16) for each damage variable as a function of the elastic energy release rate ($Y_+ = \frac{1}{2} k_i < q_i >_+^2$ and $Y_- = \frac{1}{2} k_i < q_i >_-^2$). d_∞ and b govern the evolution of the threshold function. Y_0 corresponds to the limit energy of the linear behaviour. These parameters characterize the global damage both in the positive and negative directions of the displacement. This assumption of taking the same value of d_∞, b, and Y_0 seems reasonable for simple modes without complex triaxial modeshape. It must be remarked here that the methodology cannot detect a damage related to torsion.

$$\varphi_+ = Y_+ - Y_0 \left(\frac{d_\infty}{d_\infty - D_i^+}\right)^{\frac{1}{b}} \leq 0 \quad | \quad \varphi_- = Y_- - Y_0 \left(\frac{d_\infty}{d_\infty - D_i^-}\right)^{\frac{1}{b}} \leq 0 \tag{16}$$

Damage evolves by respecting the Kuhn-Tucker conditions. By considering the condition $\varphi_i = 0$ when damage evolves, the damage evolution law can be derived (Eq. (17)).

$$D_i^+ = d_\infty \left[1 - \left(\frac{Y_0}{Y_+}\right)^b\right] \quad | \quad D_i^- = d_\infty \left[1 - \left(\frac{Y_0}{Y_-}\right)^b\right] \tag{17}$$

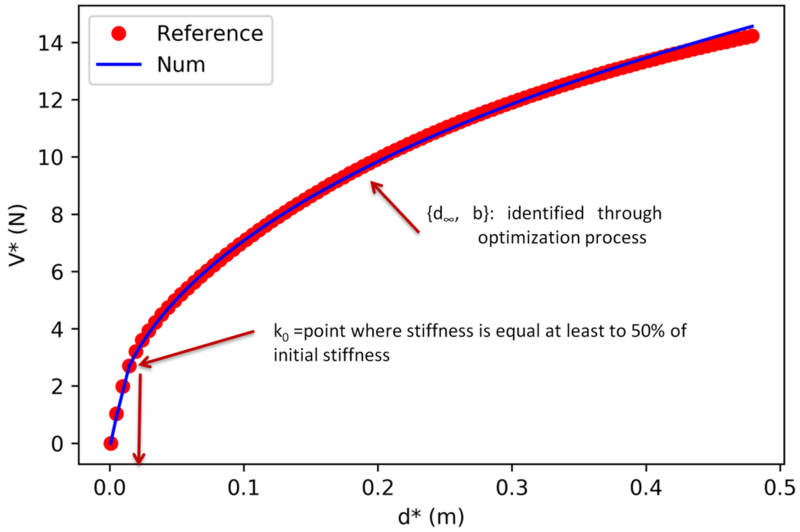

Figure 4: Example of identification of the SDOF nonlinear model for one mode.

2.3.2. *Model identification*

From the nonlinear response (V_{b_k}, q_i) of the full 3D model of the structure (see section 2.2.3), the parameters Y_0, d_∞, and b of the single degree of freedom model for mode i can be identified. The error between the response obtained by the damage model for the SDOF system and the response of the 3D model is minimized using the least-square method. Figure 4 displays the identification process, with $V^* = V_{b_k}/p_{i_k}$ and $d^* = q_i$. Figure 5 summarizes the modelling strategy, from the identification of a structural typology to the identification of the SDOF behaviour.

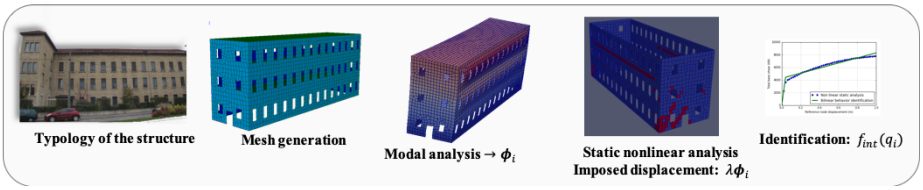

Figure 5: Modelling strategy.

2.4. *Modal recombination*

The time history analysis of the structure subject to a seismic loading is carried out on the modal basis. In order to limit the number of 3D non-linear analysis, only the first main modes are considered as non-linear. The higher modes are assumed to remain linear, with properties directly obtained from the modal analysis of the 3D structure.

Once the parameters governing the behaviour of the SDOF systems are identified for each mode, their response to a seismic loading can be easily computed by following Eq. (7). The integration method is the classical Newmark method. The non-linear equations are solved using a Newton-Raphson procedure. The displacement of each point of the structure is then obtained by modal recombination of the computed responses. This simplified modelling allows to get a complete response of a structure using few computational resources.

2.5. Damage state indicator

In order to build fragility curves for existing structures, a relevant damage indicator needs to be defined. The damage model chosen to compute the SDOF oscillator response allows to easily compute a criterion based on frequency shift, called the Eigen-Frequency Drop Off (EFDO). In this way, it is not necessary to compute the global behaviour of the structure using the modal recombination. This indicator is common to detect global damage of a structure [31]. Its relevancy has been evidenced by experimental testing [32].

The damaged frequency f_D^i of mode i and the damage level D corresponding to a frequency shift Δf are obtained with Eq.(18). D is the maximum damage level reached by mode i ($D = \max\left[D_i^+, D_i^-\right]$). f_0^i is the non damaged frequency of mode i.

$$f_D^i = \sqrt{1-D} f_0^i \;\mid\; \Delta f = \frac{f_0^i - f_D^i}{f_0^i} \;\rightarrow\; D = 2\Delta f - \Delta f^2 \tag{18}$$

The results of an analysis carried out on a SDOF equivalent oscillator are shown in figure 6. It is interesting to note that the damage variable evolves through time. This leads to a shift in the frequency response of the structure that can be seen by comparing the peaks of the fast Fourier transform (FFT) for the elastic response and the non-linear response. The FFT is carried out on the displacement of the SDOF system. For this example, the evolution of damage of the SDOF oscillator leads to an EFDO equal to 70%. The advantage of the adopted damage model is that some softening can be considered as well as an evolution in the damage law. As expected, damage is concentrated in the strong motion phase of the signal, approximately between 5s and 10s. A simple windowing algorithm can be used to calculate the EFDO for each oscillator and then for each frequency. It has been observed that higher frequency modes are less prone to step into a damaged state, because a small amount of energy is introduced by the earthquake in this frequency range. This is why the results will focus on the EFDO of the main longitudinal and transversal modes. It has been also observed that, in the vast majority of cases, damage concentrates in the first and second modes. The EFDO of higher modes is then a less interesting indicator of structural performance, although it might be an evidence of possible local phenomena activation.

The damage state 0 (DS0), characterized by negligible to slight damage (EMS98 description [33]) is defined by a range from 0% EFDO up to 15% EFDO (Limit State 1 – LS1). The average damage map observed with the pushover analysis for LS1 corresponds to distributed cracks that do not affect at all the integrity of the structure. This 15% EFDO criterion for reaching LS1 is consistent with results obtained by shaking table tests on masonry houses. For example, [32] obtained a drop in frequency of 11%

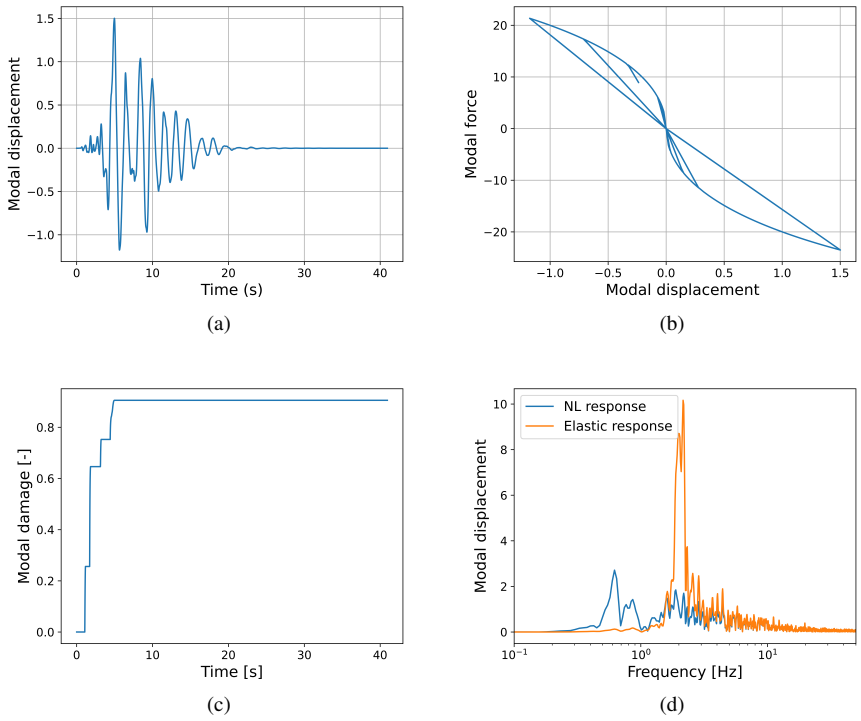

Figure 6: NLTHA of a SDOF oscillator: 6(a): displacement vs time response, 6(b): force vs. displacement response 6(c): damage evolution. 6(d): identification of the EFDO by means of a FFT calculated for the elastic oscillator (orange) and on the non linear one (blue).

for the calcium silicate masonry structure and 18% for the clay masonry structure, at the beginning of the nonlinear phase of the behaviour. [34] observed a frequency drop off of 19 % at the beginning of the first damage limit state (denoted by DL2 in [34]). For DS1 (15% to 30% EFDO), cracks are more widely distributed on the buildings, corresponding to moderate damage (EMS98 description [33]). This corresponds to an intermediate limit state between the DL2 and DL3, as defined by [34]. For larger damage states, the authors recommend to consider other modelling strategies (e.g. Structural Element Method or Macro Blocks Method [5]), that better describe the occurrence of mechanisms associated to large macro-cracks. Nevertheless, these damage states are not expected to occur for the earthquake intensities considered. Figure 7 describes the damage states for the response of a SDOF calculated directly with the damage variable (Eq. (18)).

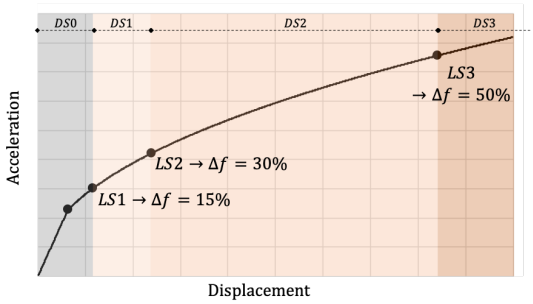

Figure 7: Definition of the damage states on the capacity curve of a SDOF (ADRS format)

3. Validation of the simplified modelling strategy

The interest of the presented approach is the possibility to perform calculations at the scale of a real structure. To illustrate this, the method is applied to a real building, from the typology shown in figure 1. This industrial building is representative of historical masonry structures built in France in the nineteenth century. This type of building is characterized by a regular shape with a homogeneous distribution of the openings and a regular story height. These simple characteristics allow to develop a parametric model with a relatively small number of parameters in order to cover a large panel of buildings in this typology.

To validate the simplified modelling strategy, one structure of the typology is considered. It is 40 meters long, for a width of 14 meters, with 3 stories of 6 meters each. Figure 8 specifies the dimensions and axes used for this reference structure. The behaviour resulting from the approach detailed in section 2 is compared to a non-linear time history analysis (NLTHA) of a 3D model of the structure. Walls are modelled with multilayer quadrangle shell elements and slabs with linear quadrangle shell elements. The multilayer shell elements have 6 layers, with 1 integration point per layer. The element size of the mesh is 60 cm. The corresponding mesh is represented in figure 9.

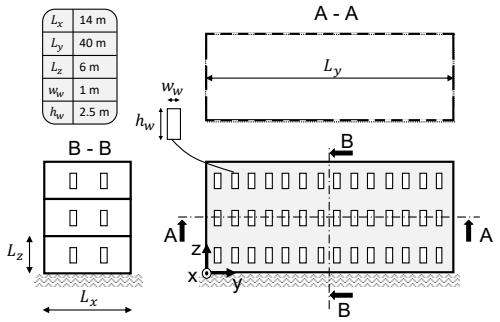

Figure 8: Geometry of the reference structure.

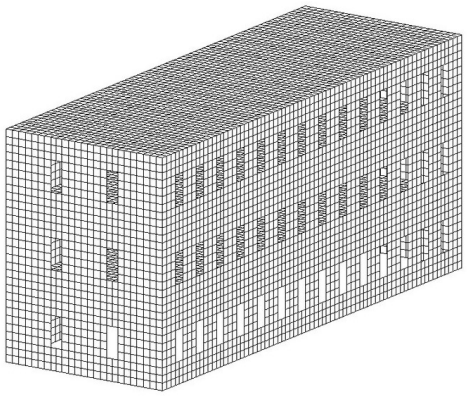

Figure 9: Mesh of the reference structure

To carry out the NLTHA, the seismic acceleration is applied as inertia forces considering a study in the relative frame. The structure is embedded at its base. Two synthetic accelerograms have been generated for this first study with target PGA of 0.1 g and 0.6 g. The method used to generate the accelerograms is detailed in section 4.2. The accelerograms have been applied to the 3D model of the structure, in the x direction (weak direction of the structure). Even though the level of acceleration of 0.6 g is too high for the purpose of the study, dedicated to low to moderate seismicity, this test case is interesting to evaluate the robustness of the proposed modelling technique for larger non-linearities.

The time-history computation of the structure is performed with the CAST3M finite element software [35]. Because of the dynamic loading, a damage model able to account for the unilateral effect needs to be used. A suitable isotropic damage model, called RICCOQ in the CAST3M software, is thus used here for the reference model. It corresponds to a simplified version of the model proposed by [36], keeping only the nonlinear mechanisms associated to damage. Its parameters have been calibrated at the material scale to provide the same average tensile behaviour curve as the Mazars damage model. The tensile strength f_t, compressive strength f_c, and the corresponding peak deformations ε_t^u and ε_c^u are given in table 1. The corresponding material parameters for the Mazars' model, described in section 2.2.2, are listed in table 2.

Model	E [GPa]	f_t [MPa]	f_c [MPa]	ε_t^u [-]	ε_c^u [-]	ρ [kg/m^3]
Unilateral	2.59	0.4	10	0.001	0.01	2500

Table 1: Material parameters of the unilateral damage model used for the masonry walls for the seismic response of the reference 3D model.

The classical Newmark time integration scheme is used, with parameters $\gamma = 1/2$, $\beta = 1/4$. A Newton-Raphson procedure is used to compute the non linear response of

Model	E [GPa]	B_T [-]	ε_{D0} [-]	ρ [kg/m^3]
Mazars	2.59 GPa	6250	0.00016	2500

Table 2: Material parameters of the the Mazars' model used for the masonry walls used in the proposed approach for the pushover-like analysis.

the structure.

As explained in section 2.3, a modal analysis is also carried out on the 3D structure. An imposed displacement following the first mode shape enables the identification of a SDOF behaviour. The corresponding force-displacement curve is displayed in figure 10. d^* is the control coefficient for the displacement, and V^* the base shear force normalized by the modal participation factor.

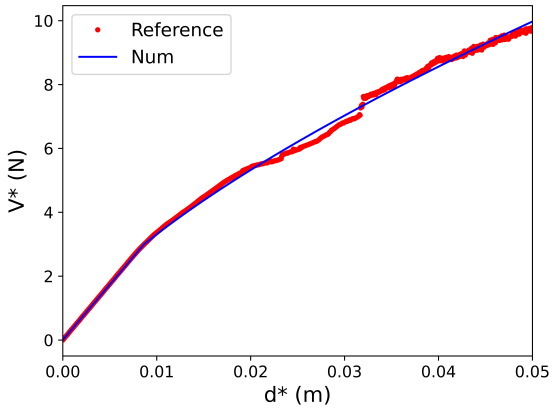

Figure 10: Identification of the nonlinear SDOF model (Num, in blue) from the global response of the pushover analysis (Reference, in red), following the procedure described in section 2.3.

The dynamic response of the Non Linear Equivalent Single Degree of Freedom (NLESDOF) oscillator is compared to the full NLTHA of the reference model. Figures 11 and 12 display the response in displacement of the middle point at the roof level and the normalized FFT of both models. The normalized FFT is obtained by dividing the FFT by the maximum of the signal. The direction of the loading has been chosen as it is the weakest direction for the building. Therefore, it corresponds to the direction in which damage develops the most. The results for three acceleration levels are presented. The response to the 0.1 g PGA seismic input has been chosen to display the results around the elastic limit. The 0.6 g PGA response corresponds to extended damage.

It can be observed in figure 11 that both models provide the same maximum displacement in the medium low acceleration domain (PGA = 0.1 g). For larger PGA (figure 12), the NLESDOF tends to overestimate the maximum displacement of the middle point at the roof level, regardless the number of modes recombined to get the

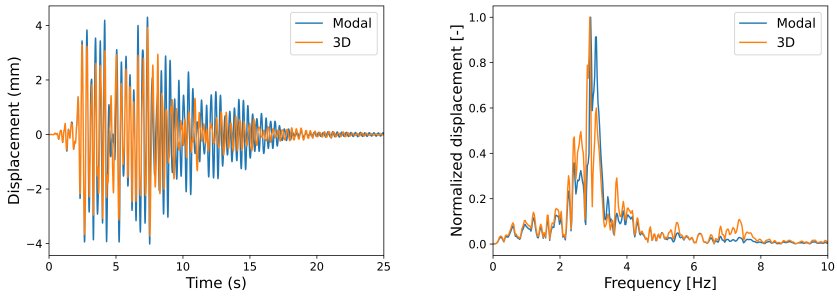

(a) (b)

Figure 11: Comparison of the responses obtained by the simplified and the global FE model, for an acceleration level of 0.1 g: displacement of the middle point at the roof level and normalized FFT.

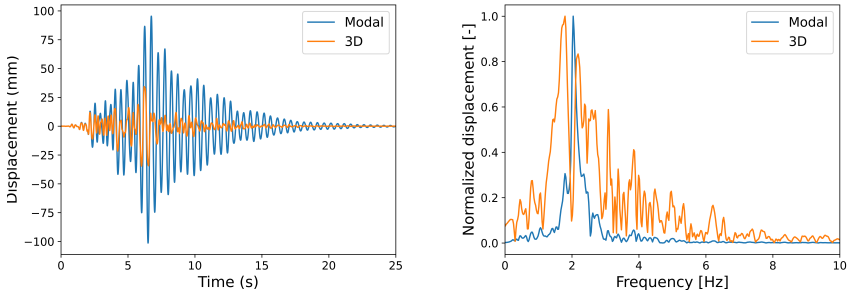

(a) (b)

Figure 12: Comparison of the responses obtained by the simplified and the global FE model, for an acceleration level of 0.6 g: displacement of the middle point at the roof level and normalized FFT.

response. This difference regarding the maximum displacement may be explained by the fact that the evolution of damping for the first mode can be observed in the 3D model considering the Rayleigh damping matrix. This effect is not considered in the NLESDOF model. In figure 13, one can see that with a modification of the damping ratio associated to the first mode (2% $\rightarrow$ 10 %), the maximum displacement is recovered with the simplified modelling. Nevertheless, without considering modification of damping ratio for the NLESDOF, one can see from the normalized FFT of the same response that the frequency drop off is well captured by the NLESDOF. The frequency drop off obtained for both models and the two signals are detailed in table 3. The damaged frequency is computed according to equation 18, using the maximum level of damage (quantified by the local damage variable D) encountered by the considered structure during the seismic loading. The NLESDOF model is so sufficiently robust to follow the damage evolution and consequently the eigenfrequency drop off up to

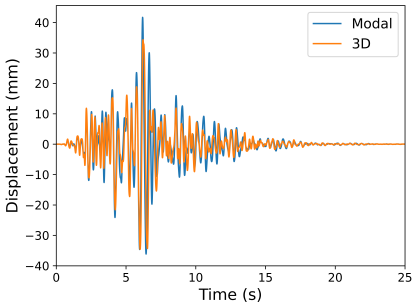

Figure 13: Comparison of the responses obtained by the simplified (with a modification of the damping) and the global FE model, for an acceleration level of 0.6 g: displacement of the middle point at the roof level and normalized FFT.

	0.1 g	0.6 g
Global FE	2%	39%
NLESDOF	2%	31%

Table 3: Eigenfrequency drop off for the global FE model and the NLESDOF for the two PGA levels.

0.6 g. This quantity is an important engineering performance indicator, that can be accurately reproduced by the simplified approach. The efficiency of the proposed numerical method enables extensive computations in a probabilistic framework, which is useful to build fragility curves.

The damage fields after the applied seismic signals corresponding to an intensity level of 0.1 g and 0.6 g are shown in figures 14 and 15 respectively. A light out-of plane flexure damage of the longitudinal walls can be observed in the case of the 0.1 g seismic loading. The damage profile of the 0.6 g case shows the activation of the in-plane shear failure mechanism in the transverse walls, starting from the window corners.

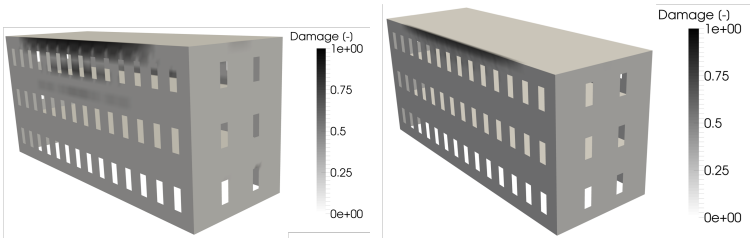

(a) (b)

Figure 14: Damage field obtained by: (a) the global FE model, (b) the pushover analysis at the maximum displacement of the NLESDOF for mode 1, for an acceleration level of 0.1 g

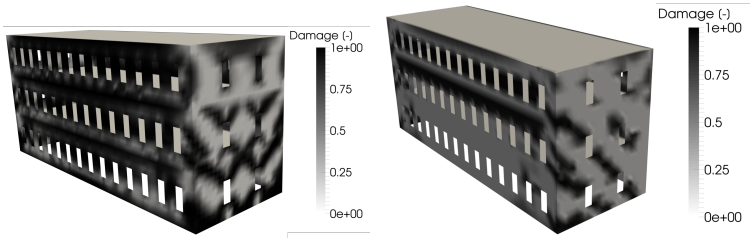

(a) (b)

Figure 15: Damage field obtained by : (a) the global FE model, (b) the pushover analysis at the maximum displacement of the NLESDOF for mode 1, for an acceleration level of 0.6 g.

Qualitatively, these damage profiles compare well with the failure modes observed in masonry shearwalls after an earthquake. Furthermore, the damage fields are comparable for the global FE model and for the damage state reached at the maximum displacement obtained with the NLESDOF for mode 1. The main difference observed for an acceleration level of 0.6 g is due to the fact that a monotonic loading is considered for the pushover analysis. As a consequence, the cracks due to shear loading are only observed for one direction (i.e. no cross crack in shear wall for monotonic loading).

4. Computation of fragility curves

4.1. Methodology

Fragility curves express the conditional probability $P_{(DS \geq DS\,i)}$ for the damage state (DS) of the structure to reach a damage state level $DS\,i$, for a given seismic intensity measure (IM), denoted by α. To compute fragility curves, damage states (DS) need to be defined, as well as the associated limit states (LS). The damage criterion is already discussed in section 2.5. For this study, a classical intensity measure is chosen with the peak ground acceleration (PGA). A synthetic seismic database has been used, as explained in section 4.2. To reduce the number of calculations of the structural response under seismic loadings, the classical lognormal fragility model is used [37]. Eq. (19) recalls the shape of the fragility curve, where Φ is the cumulative distribution function of the standard normal distribution.

$$P_{(DS \geq DS\,i)}(\alpha) = \Phi\left(\frac{ln(\alpha/A_m)}{\beta}\right) \tag{19}$$

The parameters are A_m the median capacity and β the logarithmic standard deviation. The computation of these two parameters is performed with the maximum likelihood method [38]. More information regarding the derivation of fragility curves can be found in [39]. The validity of the lognormal fragility model is analysed in section 4.3. The methodology is applied to derive fragility curves for the industrial building typology.

4.2. *Seismic database*

To compute the fragility curves, a synthetic seismic ground motion database is considered. The signals are characterized by their Power Spectral Density (PSD) [40, 41], which is a filtered white noise parameterised by the central frequency and the bandwidth. Uncertainty is accounted for by considering that the fundamental frequency f_0 follows a lognormal distribution. For this study, the mean value is set to 5 Hz. The coefficient of variation is taken equal to 10%. The bandwidth is characterized by the critical damping ratio of the filter. It is considered fixed for the PSD model and equal to 0.5. The PSD is corrected for the low frequencies with a high-pass filter at a frequency 0.1 Hz [42]. Finally, the shape of the accelerogram in the time domain is obtained with a Gamma modulation function, parameterised by the strong motion duration [43]. The mean value of the strong motion duration is equal to 9 seconds with a coefficient of variation equal to 10%. The start of the strong motion part for the modulation function is equal to 3 s.

4.3. *Analysis of the fragility curve model*

In order to validate the choice of the lognormal fragility model, a set of 2000 synthetic accelerograms is used, regularly distributed by packet of 100 each 0.05 g from 0.005 g up to 1 g. To compute a reference fragility curve, the response of a NLSDOF structure is computed using these signals. Using the maximum damage experienced by the structures, the EFDO is obtained (Eq. 18). Figure 16 shows the EFDO computed for each accelerogram of the database.

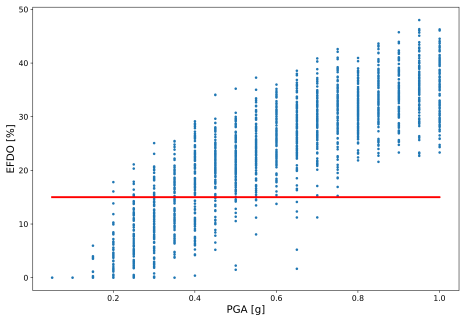

Figure 16: Cloud data representing the damage measure (EFDO) vs. the intensity measure (PGA). The 15% EFDO criterion is materialised by the red line.

This set is used to explicitly compute points of the fragility curve for an EFDO criteria of 15%. Figure 17 shows these point estimates as well as the lognormal fragility curve identified by maximum likelihood estimation (MLE).

As can be seen in figure 17, a very good agreement is obtained between the discrete points obtained by direct computation and the lognormal model. This confirms the relevance of using this model for the fragility analysis carried out in this study.

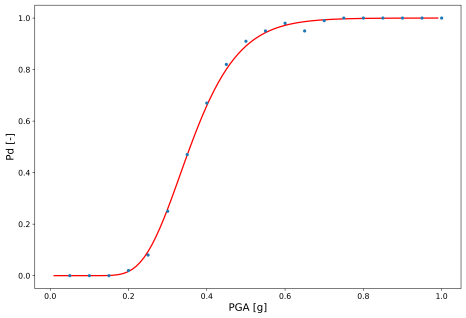

Figure 17: Discrete points and lognormal fragility curve.

Before computing fragility curves for the masonry buildings, a convergence analysis of the lognormal fragility model versus the number of synthetic accelerogram is performed. For this analysis, subsets of accelerograms are randomly picked in a database of 2900 accelerograms with PGA from 0.04 g up to 2.3 g. Figure 18 shows the probability density of the pga for the synthetic database created for the study. One can see a relative uniform distribution up to 1.5 g.

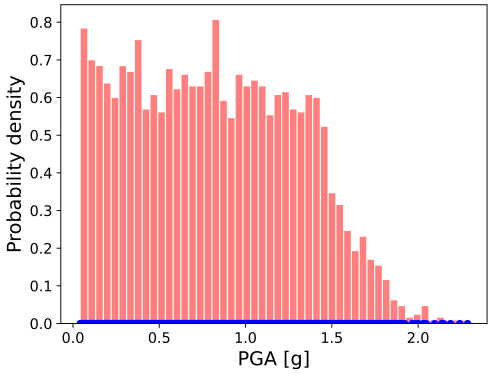

Figure 18: Probability density of the pga for the synthetic database.

Each sample of accelerograms is defined by picking signals randomly in N_s regularly distributed subsets with N_s equal to the sample size. For the convergence analysis, ten different sampling are considered for each sample size. The distribution of the value identified by MLE for the median capacity A_m and the logarithmic standard deviation β versus the sample size is studied. Figures 19 and 20 show the decrease of the standard deviation of the estimates and the convergence for β and Am respectively. In accordance with these results, a sampling size of 500 seismic signals has been adopted for

the last part of this study.

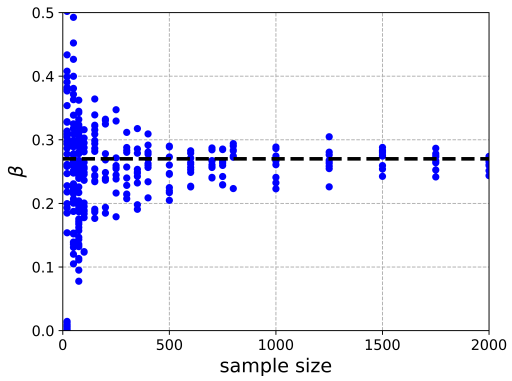

Figure 19: Evolution of the distribution of β according to the sample size.

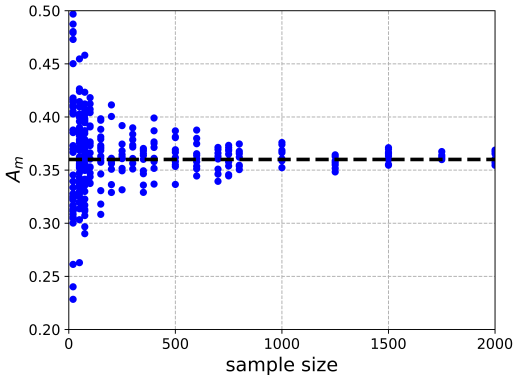

Figure 20: Evolution of the distribution of A_m according to the sample size.

4.4. Derivation of fragility curves for a building typology

The fragility model described and analysed above is used here to compute fragility curves for the industrial building typology. The global methodology to build fragility curves for a given typology is summarized in figure 21.

In order to consider the uncertainties in the characteristics of structures and materials, a probabilistic approach is adopted. Monte Carlo simulation is chosen. Each building is defined by the size of a story (length Ly, width Lx, and height Lz). All the random parameters are considered to be log-normally distributed. Table 4 summarizes the random parameters used for the industrial building typology, with their mean μ and

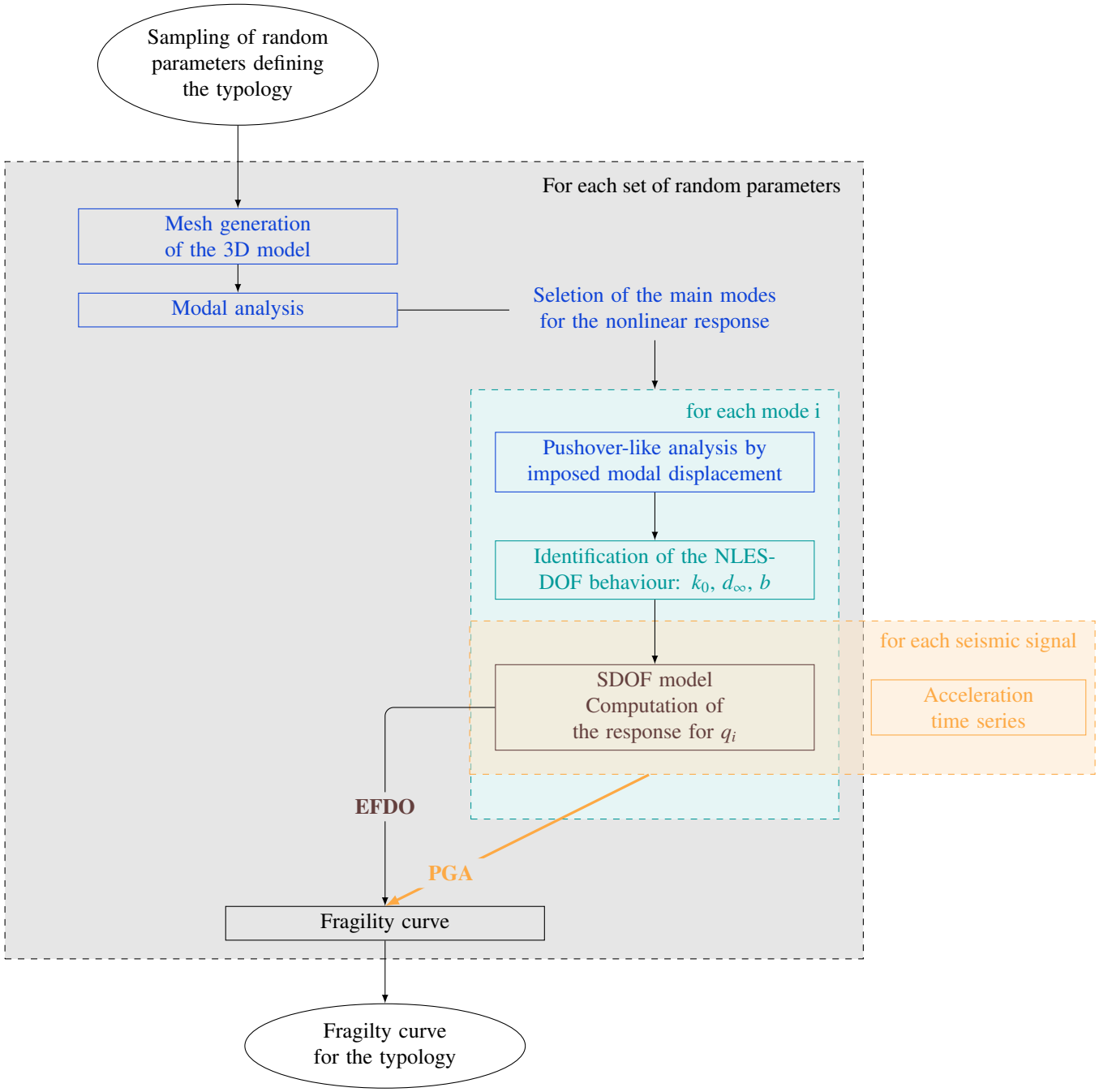

Figure 21: Global methodology to obtain the set of fragilty curves for one typology.

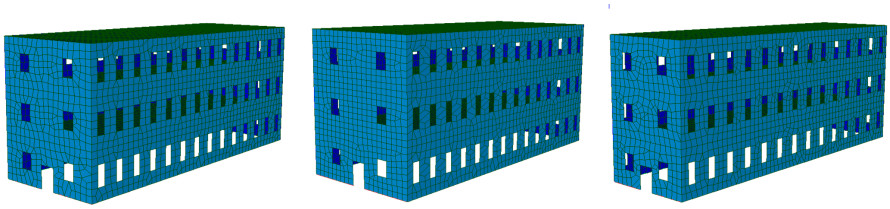

Figure 22: Geometrical mesh support: random generation of 3 models.

coefficient of variation COV values. Each building has three stories. The location and size of the openings are related to the length and width of the building.

Wood floors are considered for the building typology. No specific information is available as regards the floor stiffness, or their connection to the walls. In the model, the connections between floors and walls are considered as rigid, and the high COV applied to the floor stiffness is intended to take these uncertainties into account. Besides, the chosen mean wood floor density is lower than the practical values, and the masonry wall density higher. The choice has been made to lump part of the floor's masses to the walls, to avoid the excitation of local vertical floor modes before the structural one.

Geometrical global parameters

	μ	**COV**
Lx	14 m	20%
Ly	40 m	20%
Lz	6 m	5%

Material parameters for the masonry walls

	μ	**COV**
Young modulus E	2.5E9 N/m^2	20%
Damage model param. B_{t1}	6250	10%
Strain limit ε_{D0}	0.00016	5%
Density ρ	2500 kg/m^3	5%

Floor parameters

	μ	**COV**
Equivalent Young modulus E	1E9 N/m^2	50%
Equivalent density ρ	100 kg/m^3	20%

Table 4: Characteristics of the random distribution for the structural parameters

The geometry and the mesh of each structure is generated using the parametric mesh generator described in section 2.2. Multilayer shell elements are used to mesh the structures. Each mesh is generated by the NETGEN mesh engine, as explained in

section 2.2.1. The mesh engine uses 3 and/or 4 nodes multilayer shell elements, DKT and DKQ, based on the "Discrete Kirchhoff" kinematics [21]. The elements have 5 layers, which corresponds to 11 integration points in the element thickness. Figure 22 displays an example of 3 randomly generated meshes for the considered building typology.

195 building models have thus been generated, corresponding to the industrial building typology. For each generated mesh, the identification procedure described in section 2 is applied. The parameters of the single degree of freedom model for the first mode along the weakest (x) axis are identified for each structure according to the process explained in section 2.3.2. This identification provides information relative to the probability density for each parameters of the single degree of freedom model: k_0 ($=\omega_0^2$), Y_0, d_∞, b, represented in figure 23. These distributions show how the uncertainties propagate from the geometrical and material parameters of the 3D model to the parameters governing the SDOF model of the first mode.

During this process of identifying the SDOF models for each oscillator, the computational effort is mainly taken by the pushover analysis. Several structures can be computed in parallel, which reduces the computation time. For this case-study, 10 computation cores have been used. Doing so, the 195 models have been generated and identified within 2 days. Once the SDOF oscillators have been identified, the seismic response is very fast to compute.

500 seismic signals are randomly generated, according to the method presented in section 4.2. Using these signals and the 195 identified SDOF models, the fragility curves ($DS \geq DS1$, for the case corresponding to a first limit state LS1=15% EFDO, and $DS \geq DS2$, for the case corresponding to the second limit state LS2=30% EFDO) are plotted in figure 24. The distribution of the value identified by MLE for the median capacity A_m and the logarithmic standard deviation β versus the sample size is shown in figures 25 and 26.

The median capacity and the shape of the presented fragility curves compare well with the ones presented in [44] for similar damage levels. [44] studied a three-story masonry building in Benevento (southern Italy). Although only the order of magnitudes of the fragility curve parameters can be compared, since the building typologies are slightly different, as well as the used damage indicator, this result seems to confirm the relevancy of the obtained fragility curves.

The dispersion in the fragility curves obtained for the considered typology shows the influence of the structural uncertainties on the fragility analysis. The set of structures is large enough to allow for an adequate representation of the variability, in order to illustrate the performance of the proposed methodology. Further studies would be required in order to evaluate the sensitivity related to each parameters.

5. Concluding remarks

An efficient modelling strategy to assess the seismic vulnerability of historical masonry buildings has been presented. In order to integrate a large number of data coming from the observations on the masonry buildings, an automatic random mesh generator has been developed. To investigate the vulnerability of these buildings for a large number of seismic scenarios, a simplified modelling strategy is proposed. A 3D FE model

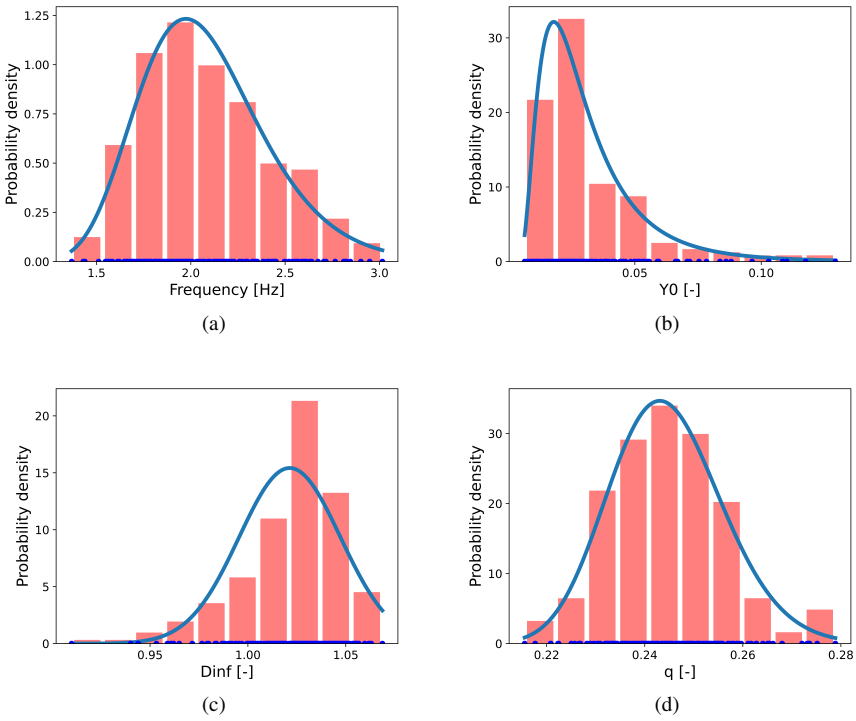

Figure 23: Probability density for : (a) f_0; (b) Y_0; (c) d_∞; (d) b.

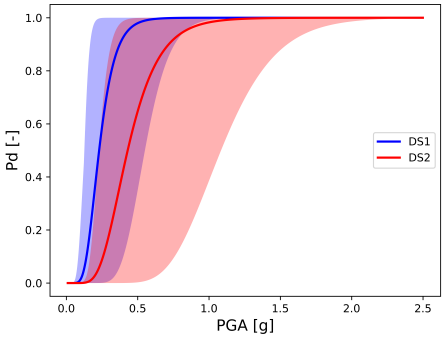

Figure 24: Fragility curves for the industrial building typology.

is built and used to determine the parameters of the NLESDOF model associated to the main modes. The nonlinear time history analysis for each earthquake loading is then performed with the simplified model. This modelling strategy has proven to be relevant

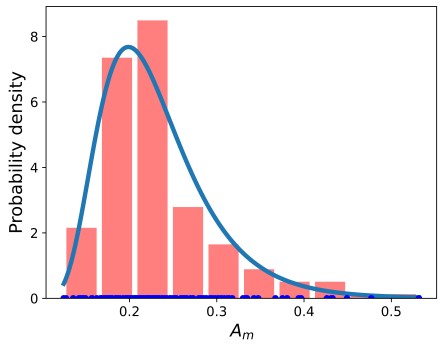

Figure 25: Median capacity A_m of the fragility curves for the industrial building typology for damage state DS1.

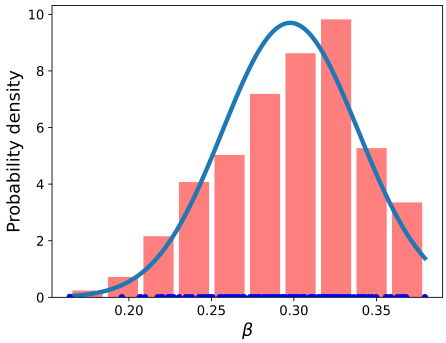

Figure 26: Standard deviation β of the fragility curves for the industrial building typology for damage state DS1.

for the identification of engineering structural response indicators, such as the maximum displacement at low level or the frequency shift. The model is valid as long as the level of damage in the structure is sufficiently low to allow the approximation of unchanged modal shapes to be relevant. It is thus an interesting approach in the context of low to moderate seismicity, when macro-modelling strategies are not adapted to model the structural behaviour. The modal basis is assumed not to be modified here, which is a reasonable assumption when the seismic loading is not too high. A comparison of the proposed strategy to a 3D full time-history analysis show that identifying the first mode enables an acccurate computation of the EFDO, chosen as a damage criterion.

The modelling strategy is applied to build fragility curves for one building typology. The case of industrial masonry buildings, representative of French constructions in the nineteenth century, is addressed. Thanks to its computational efficiency, the method can be applied to several typologies to cover a large panel of data available from in-situ observations. More case-studies can be addressed in the future, to further address the

advantages and drawbacks of the proposed modelling strategy. It would be interesting to compare the results of the proposed approach to other modelling strategy, such as the one used in "3-walls" [45]. Structural typologies for which fragility curves have already been derived, such as the ones proposed by the SYNER-G project [6], could be addressed with the proposed method for low damage levels. Sensitivity analyses on the mechanical and geometrical variables can also be conducted in order to identify the most relevant parameters, and then to eventually reduce the number of computations. In particular, it would be interesting to further investigate the influence of the floor stiffness and of the floor to wall connections on the resulting fragility curves. Once the statistical distribution of the resulting parameters of simple oscillators identified for a typology is characterized, new oscillators corresponding to the typology could also be randomly drawn to complete the set of fragility curves, taking advantage of the very fast computation of their seismic response. The derivation of fragility curves for different typologies is a step towards the update of historical earthquake intensities by a probabilistic approach.

Acknowledgements

The contribution of Alessandro Stocchi in this research was funded by EDF in the scope of the international project SIGMA2.
This work was performed using HPC resources from the "Mésocentre" computing center of CentraleSupélec and École Normale Supérieure Paris-Saclay supported by CNRS and Région Île-de-France (http://mesocentre.centralesupelec.fr/).

References

[1] H. Ryu, J. K. Kim, J. W. Baker, A probabilistic method for the magnitude estimation of a historical damaging earthquake using structural fragility functions, Bulletin of the Seismological Society of America 99 (2A) (2009) 520–537.

[2] L. Abrahamczyk, J. Schwarz, T. Langhammer, M. C. Genes, M. Bikçe, S. Kaçin, P. Gülkan, Seismic risk assessment and mitigation in the antakya–maras region (seramar): Empirical studies on the basis of ems-98, Earthquake Spectra 29 (3) (2013) 683–704.

[3] L. Abrahamczyk, T. Langhammer, J. Schwarz, Vulnerability assessment of large building stocks–lessons from the seramar project, in: 16th World Conference on Earthquake, 16WCEE2017, 2017.

[4] P. Roca, M. Cervera, G. Gariup, et al., Structural analysis of masonry historical constructions. classical and advanced approaches, Archives of Computational Methods in Engineering 17 (3) (2010) 299–325.

[5] S. Lagomarsino, H. Modaressi, K. Pitilakis, V. Bosiljkov, C. Calderini, D. D'Ayala, D. Benouar, S. Cattari, Perpetuate project: the proposal of a performance-based approach to earthquake protection of cultural heritage, in: Advanced Materials Research, Vol. 133, Trans Tech Publ, 2010, pp. 1119–1124.

[6] K. Pitilakis, H. Crowley, A. Kaynia, SYNER-G: typology definition and fragility functions for physical elements at seismic risk, Vol. 27, Springer, 2014.

[7] A. Penna, S. Lagomarsino, A. Galasco, A nonlinear macroelement model for the seismic analysis of masonry buildings, Earthquake Engineering & Structural Dynamics 43 (2) (2014) 159–179.

[8] A. Formisano, A. Marzo, Simplified and refined methods for seismic vulnerability assessment and retrofitting of an italian cultural heritage masonry building, Computers & Structures 180 (2017) 13–26.

[9] P. G. Asteris, M. Chronopoulos, C. Chrysostomou, H. Varum, V. Plevris, N. Kyriakides, V. Silva, Seismic vulnerability assessment of historical masonry structural systems, Engineering Structures 62 (2014) 118–134.

[10] M. Valente, G. Milani, Damage assessment and collapse investigation of three historical masonry palaces under seismic actions, Engineering Failure Analysis 98 (2019) 10–37.

[11] F. Minghini, G. Milani, A. Tralli, Seismic risk assessment of a 50 m high masonry chimney using advanced analysis techniques, Engineering Structures 69 (2014) 255–270.

[12] A. Formisano, G. Vaiano, F. Fabbrocino, G. Milani, Seismic vulnerability of italian masonry churches: The case of the nativity of blessed virgin mary in stellata of bondeno, Journal of Building Engineering 20 (2018) 179–200.

[13] G. Cundari, G. Milani, G. Failla, Seismic vulnerability evaluation of historical masonry churches: Proposal for a general and comprehensive numerical approach to cross-check results, Engineering Failure Analysis 82 (2017) 208–228.

[14] G. Milani, G. Venturini, Automatic fragility curve evaluation of masonry churches accounting for partial collapses by means of 3d fe homogenized limit analysis, Computers & Structures 89 (17-18) (2011) 1628–1648.

[15] B. Silva, J. M. Guedes, A. Arêde, A. Costa, Calibration and application of a continuum damage model on the simulation of stone masonry structures: Gondar church as a case study, Bulletin of Earthquake Engineering 10 (1) (2012) 211–234.

[16] G. Borino, G. Cottone, F. Parrinello, A microplane model for plane-stress masonry structures, in: Computational Fluid and Solid Mechanics 2003, Elsevier, 2003, pp. 115–117.

[17] L. Gambarotta, S. Lagomarsino, Damage models for the seismic response of brick masonry shear walls. part ii: the continuum model and its applications, Earthquake engineering & structural dynamics 26 (4) (1997) 441–462.

[18] P. B. Lourenço, J. G. Rots, J. Blaauwendraad, Continuum model for masonry: parameter estimation and validation, Journal of structural engineering 124 (6) (1998) 642–652.

[19] A. K. Chopra, R. K. Goel, A modal pushover analysis procedure for estimating seismic demands for buildings, Earthquake engineering & structural dynamics 31 (3) (2002) 561–582.

[20] L. Tataie, M. Brun, J.-M. Reynouard, Modal pushover procedures for seismic evaluation of reinforced concrete structures: using new nonlinear single degree of freedom systems, European Journal of Environmental and Civil Engineering 16 (2) (2012) 178–203.

[21] EDF, Opencascade. salome: The open source integration platform for numerical simulation (2010).

[22] C. Limoge-Schraen, C. Giry, C. Desprez, F. Ragueneau, Toward a large-scale seismic assessment method for heritage building: vulnerability of masonry baroque churches, European Journal of Environmental and Civil Engineering 20 (6) (2016) 680–710.

[23] J. Rojon, L'industrialisation du bas-dauphiné, le cas du textile (fin xviiie siècle à 1914), Ph.D. thesis, Lyon 2 (2007).

[24] G. Poursoulis, Rapport de mission réponse à la demande concernant: Etude architecturale, amélioration de la connaissance du séisme de 1889, localisation supposée à la tour du pin, Tech. rep., Archéosismicité - La mémoire des lieux (2017).

[25] J. Mazars, A description of micro-and macroscale damage of concrete structures, Engineering Fracture Mechanics 25 (5) (1986) 729–737.

[26] E. de France, Finite element *code_aster*, analysis of structures and thermomechanics for studies and research, Open source on www.code-aster.org (1989–2017).

[27] L. Facchini, M. Betti, R. Corazzi, V. C. Kovacevic, Nonlinear seismic behavior of historical masonry towers by means of different numerical models, Procedia engineering 199 (2017) 601–606.

[28] G. Bartoli, M. Betti, A. Vignoli, A numerical study on seismic risk assessment of historic masonry towers: a case study in san gimignano, Bulletin of Earthquake Engineering 14 (6) (2016) 1475–1518.

[29] P. B. Lourenço, D. V. Oliveira, J. C. Leite, J. Ingham, C. Modena, F. Da Porto, Simplified indexes for the seismic assessment of masonry buildings: International database and validation, Engineering Failure Analysis 34 (2013) 585–605.

[30] F. Minghini, E. Bertolesi, A. Del Grosso, G. Milani, A. Tralli, Modal pushover and response history analyses of a masonry chimney before and after shortening, Engineering Structures 110 (2016) 307–324.

[31] O. Salawu, Detection of structural damage through changes in frequency: a review, Engineering structures 19 (9) (1997) 718–723.

[32] C. Michel, B. Zapico, P. Lestuzzi, F. J. Molina, F. Weber, Quantification of fundamental frequency drop for unreinforced masonry buildings from dynamic tests, Earthquake Engineering & Structural Dynamics 40 (11) (2011) 1283–1296.

[33] G. Grünthal, European macroseismic scale 1998, Tech. rep., European Seismological Commission (ESC) (1998).

[34] F. Graziotti, U. Tomassetti, S. Kallioras, A. Penna, G. Magenes, Shaking table test on a full scale urm cavity wall building, Bulletin of earthquake engineering 15 (12) (2017) 5329–5364.

[35] A. Millard, Castem 2000 user manual, Tech. Rep. Rapport CEA-LAMBS No 93/007, Commissariat Francais Energie Atomique, Saclay, France (1993).

[36] R. Faria, X. Oliver, A Rate Dependent Plastic-Damage Constitutive Model for Large Scale Computations in Concrete Struktures: Monografia, Centro internacional de Métodos Numéricos en ingenieria, 1993.

[37] J. W. Reed, R. P. Kennedy, Methodology for developing seismic fragilities, Final Report TR-103959, EPRI.

[38] M. Shinozuka, M. Q. Feng, J. Lee, T. Naganuma, Statistical analysis of fragility curves, Journal of engineering mechanics 126 (12) (2000) 1224–1231.

[39] I. Zentner, M. Gündel, N. Bonfils, Fragility analysis methods: Review of existing approaches and application, Nuclear Engineering and Design 323 (2017) 245–258.

[40] K. Kanai, Semi-empirical formula for the seismic characteristics of the ground, Bulletin of the Earthquake Research Institute, University of Tokyo 35 (2) (1957) 309–325.

[41] H. Tajimi, A statistical method of determing the maximum response of a building structure during an earthquake., in: Proc. 2nd World Conf. Earthq. Eng., 1960, pp. 781–797.

[42] R. Clough, J. Penzien, Dynamics of structures, 1975, Journal of Structures, New York, McGraw-Hill Companies.

[43] S. Rezaeian, A. Der Kiureghian, Simulation of orthogonal horizontal ground motion components for specified earthquake and site characteristics, Earthquake Engineering & Structural Dynamics 41 (2) (2012) 335–353.

[44] M. Rota, A. Penna, G. Magenes, A methodology for deriving analytical fragility curves for masonry buildings based on stochastic nonlinear analyses, Engineering Structures 32 (5) (2010) 1312–1323.

[45] S. Lagomarsino, A. Penna, A. Galasco, S. Cattari, Tremuri program: an equivalent frame model for the nonlinear seismic analysis of masonry buildings, Engineering structures 56 (2013) 1787–1799.